PERGAMON

International Journal of Multiphase Flow 28 (2002) 1787–1800

International Journal of Multiphase Flow

www.elsevier.com/locate/ijmulflow

Motion of a sphere down a rough plane in a viscous fluid

Yu. Zhao [a], Kevin P. Galvin [b], Robert H. Davis [a,*]

[a] *Department of Chemical Engineering, University of Colorado, Boulder, CO 80309-0424, USA*
[b] *Department of Chemical Engineering, Centre for Multiphase Processes, University of Newcastle, Callaghan, NSW 2308, Australia*

Received 10 October 2001; received in revised form 3 July 2002

Abstract

When a sphere moves in a viscous fluid down an artificially roughened inclined plane with multiple roughness scales, its motion can be described as four successive stages: (i) descending toward the plane while in contact with a large asperity, (ii) descending toward the plane without contact, (iii) contacting the plane on small asperities, and (iv) ascending from the plane while in contact with a second large asperity. This process was analyzed by theory and experiment to provide the time variation of the translational and rotational velocities of the sphere and of its hydrodynamic separation from the plane. The translational velocity decreases weakly as the sphere descends toward the plane without contact, while the rotational velocity is nearly constant. When contact occurs, the translational velocity generally decreases, while the rotational velocity generally increases, due to solid–solid friction. For large angles of inclination of the plane from horizontal, or when the larger asperities are closely spaced or have large heights, then contact with the small asperities does not occur and the motion is dominated by contact with the large asperities and by no contact.

Keywords: Fluid mechanics; Hydrodynamic interactions; Particles; Surface roughness

1. Introduction

Interactions between particles and surfaces in a viscous fluid are of great interest in industry and academia, particularly due to their applications in composite materials processing, suspension flow, wet granular flow, and modern biotechnology (e.g., Hammer and Apte, 1992; Alon et al., 1995; Kuo et al., 1997). The critical study of sphere–plane interactions in viscous fluids includes

* Corresponding author. Tel.: +1-303-492-7314; fax: +1-303-492-4341.
E-mail address: robert.davis@colorado.edu (R.H. Davis).

0301-9322/02/$ - see front matter
PII: S0301-9322(02)00077-0

the early work of Reynolds (1886), in which he predicted that two approaching smooth surfaces never physically contact under the action of finite applied forces, due to the lubrication resistance of the intervening fluid. However, this prediction has been recently questioned from both experimental and theoretical viewpoints.

Arp and Mason (1977) observed that, with the existence of small surface roughness, two particles close together in a shearing slow rotated as a pair when in contact, and then separated, which broke the closed orbits predicted for smooth particles at low Reynolds number. Parsi and Gadala-Maria (1987) found that the pair-distribution function for sheared suspensions have different values on the approaching and receding sides of a reference sphere, in violation of the principle of reversibility for creeping flow of smooth spheres. Rampall et al. (1997) made direct measurements of the pair-distribution function in simple shear flow of dilute suspensions and found a depletion of bound pairs in the plane of shear and asymmetry in the fore and aft regions of the two-particle interactions; these observations were shown to be consistent with a simple model which includes the effects of particle surface roughness and irreversible contacts. Furthermore, in the experiments of Tabatabaian and Cox (1991), particle contacts broke the symmetry of the relative trajectory of two spheres in shear flow. In similar experiments for a pair of spheres interacting due to gravitational motion, Zeng et al. (1996) and Zhao and Davis (2002) found that the relative trajectory is affected by the size of the asperities on the sphere surfaces and the coefficient of solid–solid friction and that surface roughness and solid–solid contacts cause the symmetry predicted for smooth spheres to be broken. Surface roughness and solid–solid contacts have also been shown to affect elastohydrodynamic collisions and rebound; when a sphere was dropped onto a wetted surface, the rebound height of the sphere significantly increased when the surface was first roughened, due to a decrease in lubrication resistance (Barnocky and Davis, 1988).

The above experimental results show that the existence of microscopic surface roughness makes possible solid–solid contact in a viscous fluid. A compressive but not tensile force is expected between the two opposing surfaces that prevents closer approach when the surfaces are pushed together and contact occurs, but it loses function when they are pulled apart. In related theoretical work, Davis (1992) showed that the contact force breaks the symmetry of the trajectories of two unequal spheres interacting in sedimentation, which leads to hydrodynamic diffusion in a dilute suspension. Similarly, da Cunha and Hinch (1996) predicted hydrodynamic diffusion coefficients for dilute suspensions of rough spheres subjected to shear flow. More recently, Wilson and Davis (2000, 2002) showed that microscopic surface roughness modifies the effective viscosity of suspensions and causes normal stress differences which are absent for suspensions of smooth spheres.

As a particular case, the motion of sphere moving down an inclined plane in a viscous fluid offers researchers a convenient tool to interpret the nature of solid–solid interactions in fluids. Goldman et al. (1967) studied theoretically the motion of a smooth, non-colloidal sphere moving parallel to a smooth planar surface in viscous fluid and developed hydrodynamic resistance functions for small separations. Smart et al. (1993) extended the theory of Goldman et al. (1967) to microscopically rough surfaces and proposed that contact occurred when the minimum separation distance between the nominal surfaces decreased to the height of the roughness elements on the surfaces. They performed experiments to measure the average translational and rotational velocities of microscopically rough spheres moving due to gravity down an inclined plane and obtained good agreement with their theory, which includes both hydrodynamic forces and a

contact-friction force. In particular, the spheres rolled without slipping for small angles of inclination of the plane from horizontal, whereas slipping occurred above a critical angle where the maximum friction was reached. Prokunin (1998, 1999) also measured the translational and rotational velocities of various spheres moving down an inclined plane in a viscous fluid; at high angles of inclination, he found the measurements to be consistent with hydrodynamic theory applied at an apparent separation significantly larger than the average surface roughness measured by profilometry. A possible explanation is that there are multiple roughness scales and that the sphere is lifted away from the plane by the larger roughness elements but descends only slowly back toward the plane when the angle of inclination of the plane from horizontal is large (King and Leighton, 1997; Galvin et al., 2001).

Galvin et al. (2001) extended the theory of Smart et al. (1993) for the motion of a sphere down an inclined plane by assuming that the sphere has two roughness scales: small bumps with sufficient surface coverage to maintain a minimum separation between the nominal surfaces and larger bumps which are more sparsely distributed. From both theory and experiments, they showed that the average separation between the nominal surfaces of the plane and the sphere increases with increasing inclination of the plane from horizontal. In the present work, we further examine sphere–plane interactions by using a well-defined surface roughness pattern on the plane. The instantaneous separation and the translational and rotational velocities of the sphere are measured as functions of position or time as the sphere moves down the plane. Considerable variation in these quantities is expected when multiple roughness heights are presented, due to the dependence of the hydrodynamic resistance functions on the sphere–plane separation and due to the variation in the contact force and torques as the sphere moves over a roughness element. In the next section, the theory of Galvin et al. (2001) is modified so that the larger roughness elements are on the plane rather than the sphere. The theory is then compared with experiments using Teflon spheres moving down patterned acrylic surfaces in a viscous fluid.

2. Theoretical development

Consider a smooth sphere of radius a and density ρ_s moving down an inclined plane in a viscous fluid of viscosity μ and density ρ at low Reynolds number. The plane has microscopic surface roughness with two characteristic roughness heights: δ_L and δ_S, with the sparse large roughness heights separated by a distance L in the direction of motion (see Fig. 1). As the sphere travels down the plane, it undergoes a varying motion with the following stages:

(i) descending motion toward the plane while in contact with a large asperity,
(ii) descending motion toward the plane without contact,
(iii) motion in contact with small asperities at constant separation, and
(iv) ascending motion from the plane in contact with a second large asperity.

These four stages are considered successively in the following subsections. Since inertia is negligible at small Reynolds number, there are no significant transients between the successive stages. Statistical information on the sphere's motion and nominal separation from the plane can be obtained by considering many sequences of these four stages, with distributions of δ_L, δ_S and L.

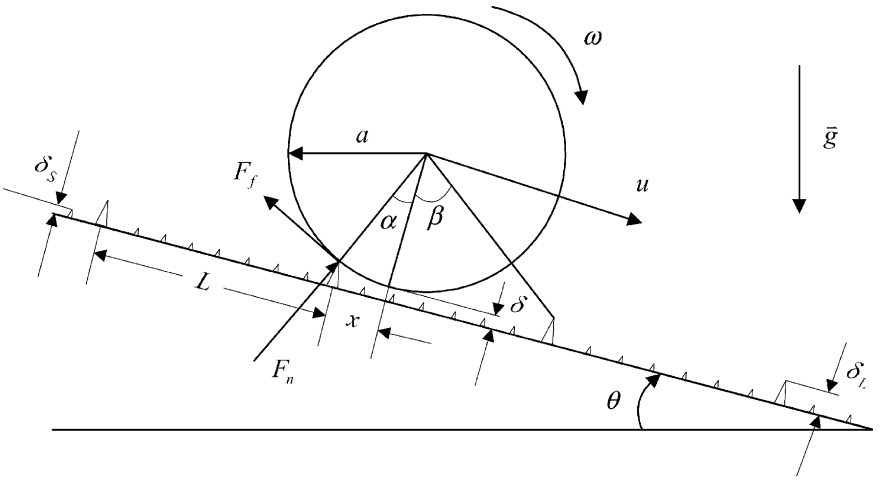

Fig. 1. Coordinate system and sketch of a sphere contacting an artificially roughened inclined plane.

2.1. Descending motion in contact with a large asperity

At $t = 0$, we consider the sphere to be located directly atop a large asperity (i.e., $\alpha = 0$, $x = 0$, $\delta = \delta_L$). If the sphere is to remain in contact with the large asperity as it translates and rotates down the plane, then it necessarily must descend toward the plane. Simple geometric constraints require that

$$\cos\alpha = 1 - (\delta_L - \delta)/a, \quad \sin\alpha = x/a, \tag{1}$$

where α is the angle between the normal to the plane and the line connecting the center of the sphere and the contact point (see Fig. 1). As the sphere descends toward the plane, its motion is resisted by a viscous lubrication force in the direction normal to the plane (Reynolds, 1886):

$$F_L = -\frac{6\pi\mu a^2}{\delta}\frac{d\delta}{dt} = \frac{6\pi\mu a^2}{\delta} u\tan\alpha, \tag{2}$$

where the second equality follows from (1), with $u = dx/dt$ as the translational velocity of the sphere down the plane.

The normal force balance on the sphere is

$$W\cos\theta = F_n\cos\alpha + F_f\sin\alpha + \frac{6\pi\mu a^2 u}{\delta}\tan\alpha, \tag{3}$$

where $W = 4\pi a^3(\rho_S - \rho)g/3$ is the net weight of the sphere in the fluid, g is the gravitational constant, F_n is the normal component of the contact force, and F_f is the frictional force. The tangential force balance on the sphere in the direction down the plane is

$$W\sin\theta = 6\pi\mu a(u\widehat{F}_t + a\omega\widehat{F}_r) + F_f\cos\alpha - F_n\sin\alpha, \tag{4}$$

where ω is the rotational velocity of the sphere and F_t and F_r are hydrodynamic resistance functions (Goldman et al., 1967):

$$\widehat{F}_{\mathrm{t}} \sim -\tfrac{8}{15}\ln\xi + 0.9588, \tag{5}$$

$$\widehat{F}_{\mathrm{r}} \sim \tfrac{2}{15}\ln\xi + 0.2526, \tag{6}$$

where $\xi = \delta/a \ll 1$ is the dimensionless separation between nominal surface of the plane and the sphere. For simplicity, we neglect any sideways motions by assuming that the large bump on the plane is aligned with equator of the sphere. Finally, the torque balance about the center of the sphere is

$$aF_{\mathrm{f}} = 8\pi\mu a^2(u\widehat{T}_{\mathrm{t}} + a\omega\widehat{T}_{\mathrm{r}}), \tag{7}$$

where the remaining hydrodynamic resistance functions for a sphere near a plane are (Goldman et al., 1967)

$$\widehat{T}_{\mathrm{t}} \sim \tfrac{1}{10}\ln\xi + 0.1895, \tag{8}$$

$$\widehat{T}_{\mathrm{r}} \sim -\tfrac{2}{5}\ln\xi + 0.3817, \tag{9}$$

valid for $\xi \ll 1$.

Following earlier work (Smart et al., 1993), we define $U = 6\pi\mu au/(W\sin\theta)$ and $\Omega = 6\pi\mu a^2\omega/(W\sin\theta)$ as dimensionless translational and rotational velocities, respectively. For rolling without slipping, $U = \Omega$, and then eliminating F_{f} and F_{n} from (3), (4) and (7) yields

$$\Omega = U = \frac{\cos\alpha + \sin\alpha\cot\theta}{(\widehat{F}_{\mathrm{t}} + \widehat{F}_{\mathrm{r}})\cos\alpha + \frac{4}{3}(\widehat{T}_{\mathrm{t}} + \widehat{T}_{\mathrm{r}}) + (\sin\alpha\tan\alpha)/\xi}. \tag{10}$$

This result is subject to $F_{\mathrm{f}} < \mu_{\mathrm{f}}F_{\mathrm{n}}$, where μ_{f} is the coefficient of friction, or

$$\cot\theta > \frac{1 + \mu_{\mathrm{f}}\tan\alpha - U[(1 + \mu_{\mathrm{f}}\tan\alpha)(\widehat{F}_{\mathrm{t}} + \widehat{F}_{\mathrm{r}}) - (\mu_{\mathrm{f}} - \tan\alpha)(\tan\alpha)/\xi]}{\mu_{\mathrm{f}} - \tan\alpha}. \tag{11}$$

When (11) is not satisfied, then the contact friction force is equal to its maximum value, $F_{\mathrm{f}} = \mu_{\mathrm{f}}F_{\mathrm{n}}$, and slipping will occur. Assuming that the coefficients of rolling and slipping friction are the same, then (3), (4) and (7) yield

$$U = \frac{\cos\alpha + \mu_{\mathrm{f}}\sin\alpha - \left(\frac{3}{4}\mu_{\mathrm{f}}\widehat{F}_{\mathrm{r}}/\widehat{T}_{\mathrm{r}} + \mu_{\mathrm{f}}\cos\alpha - \sin\alpha\right)\cot\theta}{(\widehat{F}_{\mathrm{t}} - \widehat{T}_{\mathrm{t}}\widehat{F}_{\mathrm{r}}/\widehat{T}_{\mathrm{r}})(\cos\alpha + \mu_{\mathrm{f}}\sin\alpha) - \left(\frac{3}{4}\mu_{\mathrm{f}}\widehat{F}_{\mathrm{r}}/\widehat{T}_{\mathrm{r}} + \mu_{\mathrm{f}}\cos\alpha - \sin\alpha\right)(\tan\alpha)/\xi}, \tag{12}$$

$$\Omega = \frac{\frac{3}{4}\mu_{\mathrm{f}}\cot\theta - U\left[\widehat{T}_{\mathrm{t}}(\cos\alpha + \mu_{\mathrm{f}}\sin\alpha) + \frac{3}{4}\mu_{\mathrm{f}}(\tan\alpha)/\xi\right]}{\widehat{T}_{\mathrm{r}}(\cos\alpha + \mu_{\mathrm{f}}\sin\alpha)}. \tag{13}$$

2.2. Descending motion without contact

We assume that there is no adhesion between the plane and the sphere, so that $F_{\mathrm{n}} \geqslant 0$. Then, loss of contact between the large bump and plane occurs when $F_{\mathrm{n}} = 0$. From (3), contact is first lost when

$$\xi = \xi_1 = U\tan\alpha/\cot\theta. \tag{14}$$

After contact ends, the sphere settles toward the plane without contact until the small asperities (or a second large asperity) are encountered. Assuming that the microscopic roughness does not affect the sphere–plane hydrodynamic interaction (Smart and Leighton, 1989), then the tangential and normal motions of the sphere are (Galvin et al., 2001):

$$\frac{\mathrm{d}X/\mathrm{d}T}{\sin\theta} = U = -\Omega\widehat{T}_\mathrm{r}/\widehat{T}_\mathrm{t} = \frac{1}{(F_\mathrm{t} - \widehat{F}_\mathrm{r}\widehat{T}_\mathrm{t}/\widehat{T}_\mathrm{r})}, \tag{15}$$

$$\mathrm{d}\xi/\mathrm{d}T = -\xi\cos\theta, \tag{16}$$

where $T = Wt/(6\pi\mu a^2)$ is the dimensionless time and $X = x/a$ is the dimensionless distance. Dividing (16) by (15) and integrating subject to $\xi = \xi_1$ from (14) at $X = X_1 \approx \sqrt{2(\xi_\mathrm{L} - \xi_1)}$ from (1) yields an implicit relationship for $\xi(X)$:

$$(X - X_1)\cot\theta = 1.656\ln\left(\frac{\ln\xi - 2.574}{\ln\xi_1 - 2.574}\right) + 0.3438\ln\left(\frac{\ln\xi - 0.6160}{\ln\xi_1 - 0.6160}\right). \tag{17}$$

2.3. Motion during contact with small asperities

The sphere will make contact with the small asperities when $\delta = \delta_\mathrm{S}$, provided that a second large asperity is not encountered first (see the next subsection). Following previous analyses (Smart et al., 1993; Galvin et al., 2001), we assume that the surface coverage of the small asperities on the plane (or sphere) is sufficiently high to support the sphere at constant separation ($\delta = \delta_\mathrm{S}$), but not so high that the hydrodynamic forces are significantly affected by surface roughness. In this case, the force and torque balances on the sphere yield (Smart et al., 1993):

$$\Omega = U = 1\Big/\left[\widehat{F}_\mathrm{t} + \widehat{F}_\mathrm{r} + \tfrac{4}{3}(\widehat{T}_\mathrm{t} + \widehat{T}_\mathrm{r})\right] \tag{18}$$

for rolling without slipping ($\mu_\mathrm{f}F_\mathrm{n} > F_\mathrm{f}$), or

$$U = \frac{1 - \mu_\mathrm{f}\cot\theta\left[1 + \tfrac{3}{4}\widehat{F}_\mathrm{r}/\widehat{T}_\mathrm{r}\right]}{[\widehat{F}_\mathrm{t} - \widehat{T}_\mathrm{t}\widehat{F}_\mathrm{r}/\widehat{T}_\mathrm{r}]}, \tag{19}$$

$$\Omega = \frac{1 - \mu_\mathrm{f}\cot\theta\left[1 + \tfrac{3}{4}\widehat{F}_\mathrm{t}/\widehat{T}_\mathrm{t}\right]}{[\widehat{F}_\mathrm{r} - \widehat{T}_\mathrm{r}\widehat{F}_\mathrm{t}/\widehat{T}_\mathrm{t}]}, \tag{20}$$

for rolling with slipping, where the hydrodynamic resistance functions are evaluated at $\xi = \xi_\mathrm{S} = \delta_\mathrm{S}/a$. Eq. (18) applies when

$$\cot\theta > \frac{\tfrac{4}{3}(\widehat{T}_\mathrm{t} + \widehat{T}_\mathrm{r})}{\mu_\mathrm{f}\left[\widehat{F}_\mathrm{t} + \widehat{F}_\mathrm{r} + \tfrac{4}{3}(\widehat{T}_\mathrm{r} + \widehat{T}_\mathrm{t})\right]}. \tag{21}$$

Note that the above results follow from those in Section 2.2 with $\alpha = 0$. Also, the analysis is the same if the small bumps are on the sphere rather than the plane (Smart et al., 1993; Galvin et al., 2001).

2.4. Ascending motion in contact with a large asperity

A second large asperity will be encountered when the following geometric conditions are met:

$$\xi = \xi_L + \cos\beta - 1, \quad X_L - X = \sin\beta, \tag{22}$$

where $X_L = L/a$ and β is the angle between the upward normal form the plane and the line from the sphere center to the contact point with the second large bump (see Fig. 1). Depending on the system parameters, contact with a second large asperity may occur with or without prior contact with the small asperities. Indeed, if

$$X_L < 2[1 - (1 - (\xi_L - \xi_S))^2]^{1/2} \approx [8(\xi_L - \xi_S)]^{1/2}, \tag{23}$$

then contact with the small asperities is not geometrically possible.

Once the sphere makes contact with the second large asperity, it will be lifted away from the plane in a 'pole-vault' fashion. The analysis of Section 2.1 still holds, except that α is replaced by $-\beta$. Note that the lubrication force from (2) is now negative, as a suction pressure develops to draw fluid into the increasing gap as the sphere ascends from the plane. The negative lubrication force in the normal force balance (3) causes a greater normal contact force, which, in turn, implies greater friction and less slip.

3. Experimental materials and methods

The experimental apparatus consists of a plexiglass tank with a cross section of 10 in. × 6 in. and a height of 6 in. (see Fig. 2), which is filled with a Newtonian fluid consisting of a mixture of 97.4% polyalklene glycol and 2.6% tetrabromoethane by weight. The temperature dependence of the fluid kinematic viscosity is represented by the equation $v = 1209\exp(-0.0547T_0)$, where v has units of cm^2/s and the temperature T_0 is expressed in °C. The fluid density is $\rho = 1.118$ g/cm^3 at $T_0 = 4$ °C and $\rho = 1.111$ g/cm^3 at $T = 25$ °C.

Several tungsten metal cleaning wires (Hamilton Co.) with a diameter of $\delta_L = 0.003$ or 0.005 in. (0.0076 or 0.0127 cm) are set parallel to each other and attached on the bottom surface of the tank to serve as the artificial roughness of the plane. The separation between two adjacent wires is set at $L = 0.125$ or 0.25 in. (0.318 or 0.635 cm). The motion of the sphere is recorded with a digital camcorder (Canon ELURA), a Digital Origin 1394 card, and a personal computer (HP 9694C).

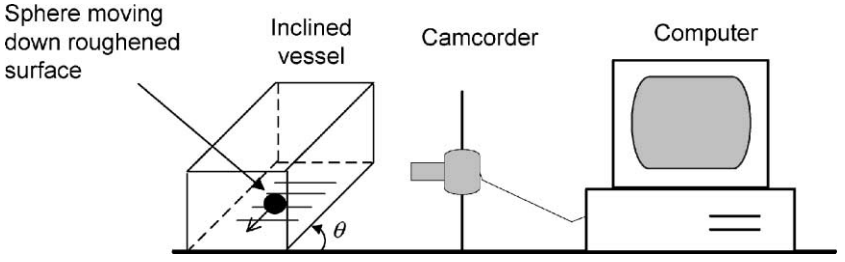

Fig. 2. Schematic of the experimental setup.

Teflon ($\rho_1 = 2.154$ g/cm^3) spheres with radius $a = 0.125$ in. (0.318 cm) are employed in the experiments. All spheres were purchased from Small Parts, Inc. They were marked with ink dots to show their rotational motions. Scanning electron micrographs of the sphere surfaces show roughness elements of about 10 μm (Galvin et al., 2001). The dry coefficients of static and sliding friction between the teflon sphere and the acrylic plane were measured as 0.19 ± 0.02 and 0.12 ± 0.01, respectively (Galvin et al., 2001). The coefficient of sliding friction between teflon and metal is approximately 0.1 (Elias, 1992), similar to that between teflon and acrylic.

In the experiments, a teflon sphere is introduced into the tank and allowed to sediment onto the horizontal bottom of the tank. After standing for 1–2 min to assure full contact between the sphere and the bottom plane of the tank, the apparatus is inclined so that the sphere moves down the plane perpendicular to the wires. Its motion is recorded by the digital camcorder and then transferred into the computer. Scion Image software (NIH Image) is used to analyze the image files to determine the translational and rotational velocities of the sphere. To measure the normal separation between the sphere and the plane, the method developed by Galvin et al. (2001) is employed. When the sphere reaches a certain position between two adjacent metal wires, the whole apparatus is inverted to make the bottom of tank horizontal and facing down. Under the action of gravity and resisted by lubrication forces, the sphere slowly falls from the its initial position. The fall process (at least two sphere diameters in vertical direction) is recorded by the digital camcorder. According to the analysis of Smart and Leighton (1989), the dimensionless initial separation is given by

$$\xi = 2\exp\left(2 - \frac{t_d}{t_d - t_a}(1 + \ln 2)\right), \tag{24}$$

where t_d and t_a are the times for the sphere to fall one diameter and one radius from its initial position, respectively.

4. Results and discussion

The theory and experiments described above yield predictions for the dimensionless nominal separation (ξ), translational velocity (U), and rotational velocity (Ω) as functions of dimensionless time (T) or distance (X) traveled down the inclined plane. The results depend on five dimensionless parameters ($\xi_S, \xi_L, X_L, \mu_f, \theta$). Fortunately, all of these parameters may be set or measured independently. In particular, for the current experiments, $\xi_L = 0.024$ or 0.040 is set by the sizes of the wires and teflon ball, $X_L = 1.0$ or 2.0 is set by the spacing of the wires, $\theta = 30°$, 50° or 70° is set by varying the angle of inclination of the plane, and $\mu_f = 0.15$ is the average coefficient of friction measured for a teflon ball rolling or sliding down an inclined acrylic surface under dry conditions (Galvin et al., 2001). The same value of μ_f was typically used when the sphere contacted the metal wires, and the results were found to depend only weakly on the value(s) chosen for μ_f. Finally, $\xi_S = 0.0016$ ($\delta_S = 5.1$ μm) was determined by allowing the teflon sphere to sediment onto a horizontal acrylic surface (without wires) and then inverting the surface and timing the sphere as it fell away from the surface.

Fig. 3 shows the dimensionless distance X and the angle ϕ versus the adjusted dimensionless time $T \sin\theta$, starting from the point that the sphere contacts the plane right on the top of a large

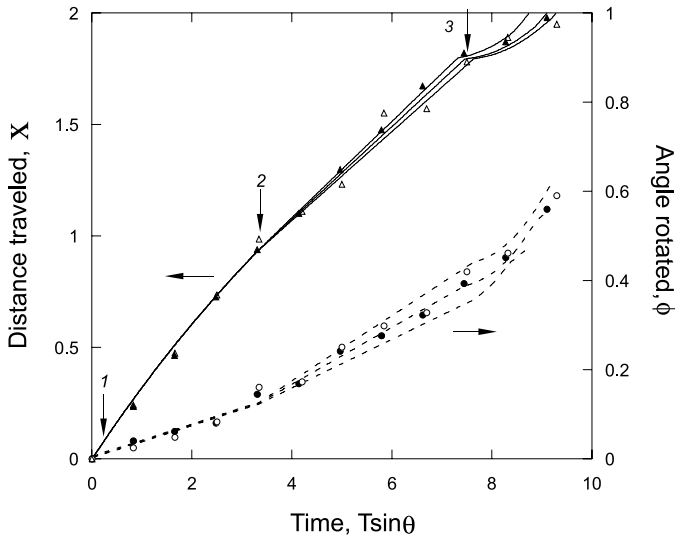

Fig. 3. Dimensionless distance X (solid lines for theory and triangles for experiments) and angle ϕ (dashed lines for theory and circles for experiments) versus the dimensionless time $T\sin\theta$ for $\theta = 50°$, $\xi_L = 0.024$, $\xi_s = 0.0016$, and $X_L = 2$. From top to bottom, the coefficients of friction used in the theoretical calculations are $\mu_f = 0.2$, 0.15 and 0.1. The arrows 1, 2 and 3 indicate when the sphere loses contact with the first large bump, when the sphere then makes contact via the small bumps, and when the sphere makes contact with the second large bump, respectively.

asperity, for $\theta = 50°$, $X_L = 2$, and $\xi_L = 0.024$. Varying the friction coefficient over the range $0.1 \leqslant \mu_f \leqslant 0.2$ has little effect on the translational velocity and only a modest effect on the rotational velocity. The arrows 1, 2 and 3 in this and subsequent figures correspond to when the sphere loses contact with the first large bump, when the sphere contacts the small bumps, and when the sphere meets the second large bump, respectively. Loss of contact with the first large bump occurs very quickly, and then the translational velocity decreases weakly while the rotational velocity is nearly constant as the sphere descends toward the plane without contact. When the small bumps are encountered, the translational velocity decreases further, while the rotational velocity increases, because of the solid–solid friction force. Finally, when the second large bump is encountered, the translational velocity is further reduced as lubrication suction resists the lifting of the sphere over the bump. These features are illustrated further in Fig. 4, which shows the dimensionless translational and rotational velocities for the same conditions. Until contact with the second large bump occurs, the dimensionless translational velocity is much greater than the dimensionless rotational velocity, indicating that slipping occurs. When the second large bump is first encountered, the dimensionless translational and rotational velocities coincide, because the large normal contact force to balance both gravity and lubrication suction allows for a large friction force which prevents slipping until the apex is nearly reached. Figs. 3 and 4 show very good agreement between theory and experiment, even though the long wires are expected to modify the hydrodynamic interactions between the sphere and the plane in the vicinity of a large bump. The open and closed symbols show good reproducibility between repeated experiments.

Fig. 5 presents the dimensionless separation ξ between the sphere and plane and the angle rotated ϕ versus the dimensionless distance traveled X, for the same conditions as in Fig. 3 except

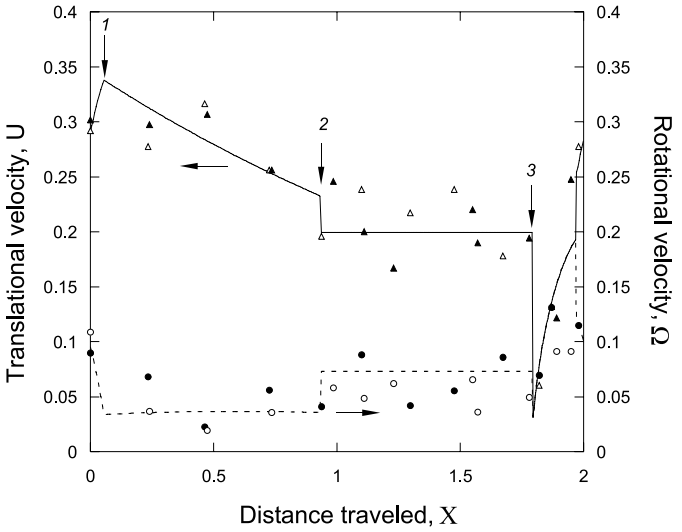

Fig. 4. Dimensionless translational velocity U (solid lines for theory and triangles for experiments) and rotational velocity Ω (dashed lines for theory and circles for experiments) versus the dimensionless distance X for the conditions of Fig. 3 with $\mu_f = 0.15$ used in the theory. The arrows 1, 2 and 3 indicate when the sphere loses contact with the first large bump, when the sphere then makes contact via the small bumps, and when the sphere makes contact with the second large bump, respectively.

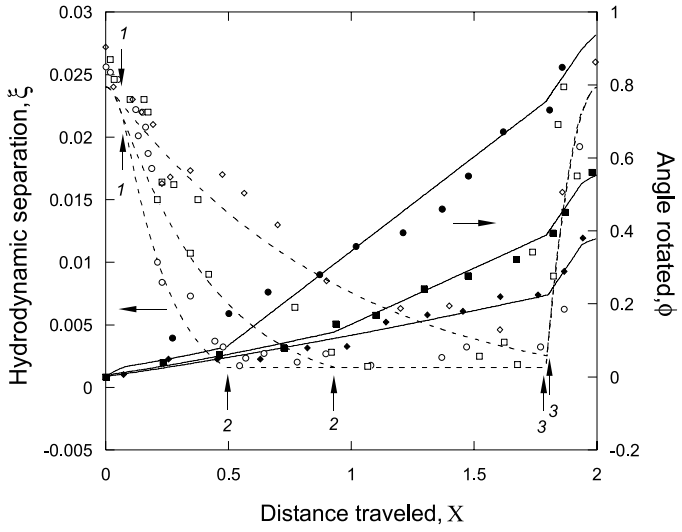

Fig. 5. Dimensionless separation ξ (dashed lines for theory and open symbols for experiments) and angle ϕ (solid lines for theory and solid symbols for experiments) versus the dimensionless distance X, for the conditions of Fig. 4 but with $\theta = 30°$ (circles), 50° (squares), and 70° (diamonds). The arrows 1, 2 and 3 indicate when the sphere loses contact with the first large bump, when the sphere then makes contact via the small bumps, and when the sphere makes contact with the second large bump, respectively.

that the angles of inclination are $\theta = 30°$, 50° and 70°. The dimensionless separation ξ decreases gradually during the period of no contact, with the motion normal to the plane resisted by lubrication, and is then nearly constant during the period of contact with the small asperities. Finally, the contact with a second large asperity provides a rapid increase in the dimensionless separation. With increasing angle of inclination of the plane from horizontal, the motion of the sphere toward the plane during the period of no contact becomes slower, due to the smaller normal component of gravity, and contact with the small bumps on the plane is not made for the largest angle investigated ($\theta = 70°$) before a second large bump is encountered. As noted previously, the rate of rotation of the sphere relative to its translation increases when the small bumps are encountered and then again when the second large bump is reached. Also, the relative amount of rotation of the sphere is greater at smaller angles, because the larger component of the gravity vector normal to the plane gives rise to higher friction during contact with the small bumps and, hence, more rotation and less slip. Fig. 6, which shows the dimensionless distance traveled and angle rotated versus time (with $\sin\theta$ included to account for the change in the tangential component of gravity with angle) for $\theta = 30°$ and 70°, further illustrates that more slip (less rotation and more translation) occurs when the steepness of the plane is increased.

Figs. 7 and 8 show results for $\theta = 50°$ when two adjacent wires are close together ($X_L = L/a = 1$) and have a dimensionless roughness height of $\xi_L = 0.024$ or 0.040. Unlike the previous cases where $X_L = 2$, the second large asperity is encountered before the sphere settles to a nominal separation equal to the height of the small asperities, which makes the average separation between the sphere and the plane closer to the size of the large asperities. Of course, the sphere–plane separation is then greater during the entire encounter when the larger wires are used to lift the

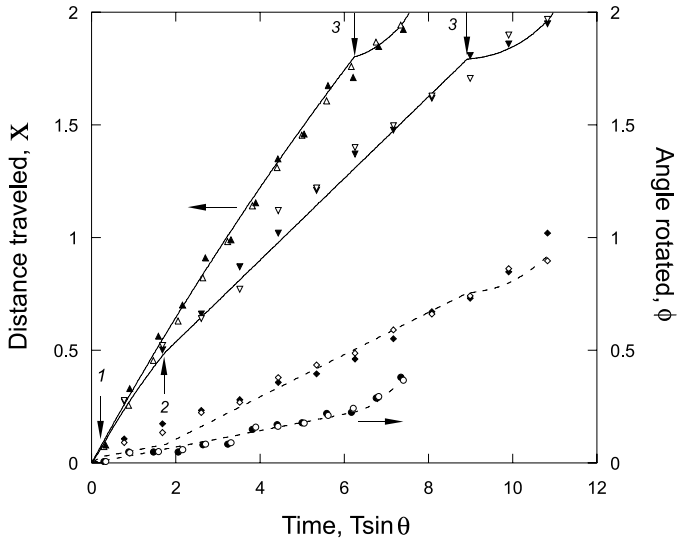

Fig. 6. Dimensionless distance X (solid lines for theory and triangles for experiments) and angle ϕ (dashed lines for theory and circles and diamonds for experiments) versus the dimensionless time $T\sin\theta$ for $\xi_L = 0.024$, $\xi_s = 0.0016$, $X_L = 2$, $\mu_f = 0.15$ and $\theta = 30°$ (top for ϕ and bottom for X) and 70°. The arrows 1, 2 and 3 indicate when the sphere loses contact with the first large bump, when the sphere then makes contact via the small bumps, and when the sphere makes contact with the second large bump, respectively.

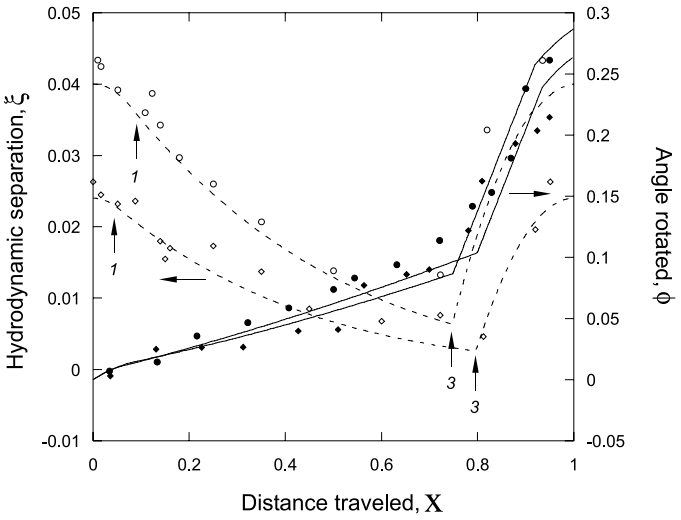

Fig. 7. Dimensionless separation ξ (dashed lines for theory and open symbols for experiments) and angle ϕ (solid lines for theory and solid symbols for experiments) versus the dimensionless distance X, for $\theta = 50°$, $\xi_S = 0.0016$, $X_L = 1$, $\mu_f = 0.15$, and $\xi_L = 0.040$ (circles) and 0.024 (diamonds). The arrows 1 and 3 indicate when the sphere loses contact with the first large bump and makes contact with the second large bump, respectively; contact with the small bumps does not occur in this case.

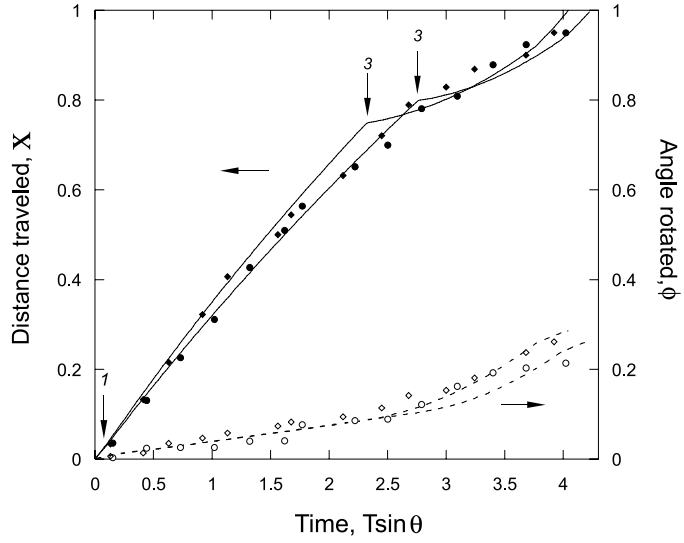

Fig. 8. Dimensionless distance X (solid lines for theory and solid symbols for experiments) and angle ϕ (dashed lines for theory and open symbols for experiments) versus the dimensionless time $T \sin\theta$, for the conditions of Fig. 7 with $\xi_L = 0.024$ (diamonds, upper line for ϕ and lower line for X) and 0.040 (circles, lower line for ϕ and upper line for X). The arrows 1 and 3 indicate when the sphere loses contact with the first large bump and makes contact with the second large bump, respectively; contact with the small bumps does not occur in this case.

sphere further from the plane, but the translational and rotational velocities of the sphere are only weakly affected by this difference.

5. Conclusions

Both theory and experiment show that a sphere experiences a time-varying motion down an inclined plane with multiple roughness scales in a viscous fluid. The contact of the sphere with the plane transitions from large bumps to small bumps, with a period of contact-free motion in between. Because of solid–solid friction, the translational velocity of the sphere decreases when contact is made, whereas the rotational velocity generally increases. Moreover, as the angle of inclination of the plane is increased, the normal component of gravity is decreased and the sphere does not settle back onto the plane to make contact with small roughness elements in between the interactions with large roughness elements which cause the sphere to rise away from the nominal surface of the plane in a pole-vault-like fashion. These findings are expected to have implications in suspension rheology and microstructure through particle-surface and particle-particle contacts due to microscopic surface roughness.

Acknowledgements

This work was supported by the US National Science Foundation through grant CTS-9712604, and by the National Aeronautics and Space Administration through grant NCC3-796.

References

Alon, R., Hammer, D.A., Springer, T., 1995. Lifetime of the P-selectin: Carbohydrate bond in response to force on neutrophils in hydrodynamic flow. Nature 374, 539–542.

Arp, A.P., Mason, S.G., 1977. The kinetics of flowing dispersions. IX. Doublets of rigid spheres (experimental). J. Colloid Interf. Sci 61, 44–61.

Barnocky, G., Davis, R.H., 1988. Elastohydrodynamic collision and rebound of spheres: experimental verification. Phys. Fluids 31, 1324–1329.

da Cunha, F.R., Hinch, E.J., 1996. Shear-induced dispersion in a dilute suspension of rough spheres. J. Fluid Mech. 309, 211–223.

Davis, R.H., 1992. Effects of surface roughness on a sphere sedimenting through a dilute suspension neutrally buoyant spheres. Phys. Fluids A 4, 2607–2619.

Elias, H.-G., 1992. Plastics, general survey. In: Ulmann's Encyclopedia of Industrial Chemistry A20, pp. 543–661.

Galvin, K.P., Zhao, Y., Davis, R.H., 2001. Time-averaged hydrodynamic roughness of a noncolloidal sphere in low Reynolds number motion down an inclined plane. Phys. Fluids 13, 3108–3120.

Goldman, A.J., Cox, R.G., Brenner, H., 1967. Slow viscous motion of a sphere parallel to a plane wall. I. Motion through a quiescent fluid. Chem. Eng. Sci 22, 637–650.

Hammer, D.A., Apte, S.M., 1992. Simulation of leukocyte rolling and adhesion on surfaces in shear flow: General results and analysis of selectin-mediated neutrophil adhesion. Biophys. J. 63, 35–57.

King, M.R., Leighton, D.T., 1997. Measurement of the inertial lift on a moving sphere in contact with a plane wall in shear flow. Phys. Fluids 9, 1248–1255.

Kuo, S.C., Hammer, D.A., Lauffenburger, D.A., 1997. Simulation of the detachment of specifically-bound particles from surfaces by shear flow. Biophys. J. 73, 517–531.

Parsi, F., Gadala-Maria, F., 1987. Fore-and-aft symmetry in a concentrated suspension of solid spheres. J. Rheol. 31, 725–732.

Prokunin, A.N., 1998. Spherical particle sedimentation along an inclined plane at small Reynolds numbers. Fluid Dyn. 23, 573–579.

Prokunin, A.N., 1999. Towards a paradox in particle motion in a fluid near a wall. In: Proc. Int. Conf. Problems in Fluid Mech. Hydrol., pp. 143–146.

Rampall, I., Smart, J.R., Leighton, D.T., 1997. The influence of surface roughness on the particle-pair distribution function of dilute suspensions of non-colloidal spheres in simple shear flow. J. Fluid Mech. 339, 1–24.

Reynolds, O., 1886. On the theory of lubrication and its application to Mr. Beauchamp Tower's experiments. Phil. Trans. Roy. Soc. London 177, 157–234.

Smart, J.R., Beimfohr, S., Leighton, D.T., 1993. Measurement of the translational and rotational velocities of a noncolloidal sphere rolling down a smooth inclined plane at low Reynolds number. Phys. Fluids A 5, 13–24.

Smart, J.R., Leighton, D.T., 1989. Measurement of the hydrodynamic surface roughness of noncolloidal spheres. Phys. Fluids A 1, 52–60.

Tabatabaian, M., Cox, R.G., 1991. Effect of contact forces on sedimenting spheres in Stokes flow. Int. J. Multiphase Flow 17, 395–413.

Wilson, H.J., Davis, R.H., 2000. The viscosity of a dilute suspension of rough spheres. J. Fluid Mech. 421, 339–367.

Wilson, H.J., Davis, R.H., 2002. Shear stress of a dilute monolayer of rough spheres. J. Fluid Mech. 452, 425–441.

Zeng, S., Kerns, E.T., Davis, R.H., 1996. The nature of particle contacts in sedimentation. Phys. Fluids 8, 1389–1396.

Zhao, Y., Davis, R.H., 2002. Interaction of two touching spheres in a viscous fluid. Chem. Eng. Sci. 57, 1997–2006.